OPEN ACCESS

Original research

Evaluation of Sine Spin flat detector CT imaging compared with multidetector CT

Valentina D Petroulia, Johannes Kaesmacher, Eike I Piechowiak, Tomas Dobrocky, Sara M Pilgram-Pastor, Jan Gralla, Franca Wagner, Pasquale Mordasini

► Additional supplemental material is published online only. To view, please visit the journal online (http://dx.doi.org/10.1136/neurintsurg-2021-018312).

Department for Diagnostic and Interventional Neuroradiology, Inselspital, Bern University Hospital and University of Bern, Bern, Switzerland

Correspondence to
Dr Pasquale Mordasini, University of Bern, Bern, Switzerland; pasquale.mordasini@insel.ch

VDP and JK contributed equally. FW and PM contributed equally.

Received 8 November 2021
Accepted 28 February 2022
Published Online First 22 March 2022

ABSTRACT

Background Flat detector computed tomography (FDCT) is widely used for periprocedural imaging in the angiography suite. Sine Spin FDCT (SFDCT) is the latest generation of cone beam CT using a double oblique trajectory for image acquisition to reduce artefacts and improve soft tissue brain imaging. This study compared the effective dose, image quality and diagnostic performance of the latest generation of SFDCT with multidetector CT (MDCT).

Methods An anthropomorphic phantom equipped with MOSFET detectors was used to measure the effective dose of the new 7sDCT Sine Spin protocol on a latest generation biplane angiographic C-arm system. Diagnostic performance was evaluated on periprocedurally acquired SFDCT for depiction of anatomical details, detection of hemorrhage, and ischemia and was compared with preprocedurally acquired MDCT. Inter- and intra-rater correlation as well as sensitivity and specificity were calculated.

Results Both modalities showed equal diagnostic performance in the supratentorial ventricular system. SFDCT provided inferior image quality in grey-white matter differentiation and infratentorial structures. Intraventricular, subarachnoid and parenchymal hemorrhages were diagnosed with a sensitivity of 83.3%, 84.2% and 75% and a specificity of 97.3%, 80.0% and 100%, respectively; early ischemic lesions with a sensitivity of 73.3% and specificity 94.7%. The effective dose measured for the 7sDCT Sine Spin protocol was 2 mSv.

Conclusions Our findings confirm the high diagnostic sensitivity and specificity of SFDCT in detecting intracranial hemorrhage and early ischemic lesions. The delineation of grey-white matter differentiation and infratentorial structures remains a limiting factor. In comparison to previous studies, the new 7sDCT Sine Spin protocol showed a lower effective dose.

To cite: Petroulia VD, Kaesmacher J, Piechowiak EI, *et al*. *J NeuroIntervent Surg* 2023;**15**:292–297.

INTRODUCTION

Initially targeted at neuroendovascular imaging of contrast-enhanced vascular structures, three-dimensional (3D) C-arm imaging has continuously improved over the years. It is now capable of providing CT-like soft tissue image quality directly in the interventional angiography suite. If C-arm systems can rotate around a patient through a sufficiently large angular scan range, then it is possible to use the acquired X-ray projections for tomographic image reconstruction, so-called cone beam flat detector computed tomography (FDCT).

However, compared with multidetector computed tomography (MDCT), conventional cone beam FDCT has limitations, especially in imaging the infratentorial structures close to the skull base, because of motion and beam hardening artefacts, and in the quality of soft tissue brain imaging. Image artefacts caused by the limited-angle CT reconstruction in cone beam CT are a significant source component for reduced image quality and therefore diagnostic accuracy. A new biplane C-arm system ARTIS icono (Siemens Healthcare GmbH, Forchheim, Germany) with the latest generation FDCT, so-called 'syngo DynaCT Sine Spin' (hereafter referred to as SFDCT), was developed to reduce artefacts from bony structures and to further improve soft tissue brain imaging. Established FDCT protocols usually require a minimum angular scan range of 180° plus the so-called fan-angle to achieve a sufficiently large angular scan range for the acquisition of X-ray projections for tomographic image reconstruction.[1] For typical C-arm FDCT devices, this results in an angular scan range requirement of 200°.[2] The new Sine Spin acquisition protocol uses a double oblique trajectory with slight craniocaudal modulation with a scan range of 220°. This allows for a potential reduction of cone beam artefacts, especially at the skull base, more precise reconstruction of the entire image volume and optimised contrast resolution to improve visualization of brain tissue.

The aim of this study was twofold. The first was to evaluate the effective dose to the patient of the SFDCT protocol and to compare it with previously published effective dose values for established FDCT protocols. The second was to compare the image quality and diagnostic accuracy of the SFDCT protocol with conventional MDCT.

MATERIALS AND METHODS

Patient selection

This was a retrospective observational study which included all patients imaged with MDCT and SFDCT (ARTIS icono biplane) in our department from March 2019 to May 2020. Patients were screened for periprocedural MDCT and SFDCT in-house within a time window of 24 hours. A total of 49 patients with complete MDCT and SFDCT scans were included in this study. The study was performed in accordance with the principles of the

Declaration of Helsinki and was approved by the local ethics committee (Kantonale Ethikkomission Bern, KEK, Basec PB 2018–02023).

Data acquisition

SFDCT imaging

The conventional syngo DynaCT neuro protocol (20sDCT Head) is a planar rotation (planar: focal spot stays within a plane) over 200° with an angular increment of 0.4°, adding up to 496 projection images. The scan is from right anterior oblique (RAO) 100 to left anterior oblique (LAO) 100, the craniocaudal angle stays at zero. In the new protocol 'syngo DynaCT Sine Spin' there is slight Cran/Caud modulation, like a sine curve, with an amplitude of 10° and the scan is over 220° from RAO 110 to LAO 110. The scan starts at −110°/0°, goes to −55°/10°, then 0°/0°, 55°/−10°, and finally to 110°/0°. The angular increment is 0.4°, adding up to 546 projections. The new protocol is offered in two variations: 7sDCT Sine Spin (with 4×4 binning and a soft reconstruction) and 9sDCT Sine Spin (with 2×2 binning and a sharper reconstruction). The first protocol is used to visualize soft tissue changes such as hemorrhage or infarction and the second is used to visualize devices (eg, stents or coils). In the present study the 7sDCT Sine Spin protocol was used and evaluated in the ARTIS icono angiography system, with all patients under general anesthesia.

MDCT imaging

MDCT scans of all subjects were performed using a 128-detector row CT scanner (SOMATOM Definition Edge; Siemens Healthcare). A standard brain scan protocol was followed as part of the routine work-up of patients in the acute setting to rule out stroke or an intracranial hemorrhage.

Images were acquired from patients in the supine position in the direction from caudal to cranial. A tube voltage of 100 kV was applied. Scans were performed with automated exposure control and tube current modulation (X CARE Z EC, Siemens Healthcare). Pixel matrix size was 512×512 mm, collimation was 128×0.6 mm, pitch was 0.6 and rotation time was 0.28 s. Second-generation iterative reconstruction (kernel J45s) was used for image reconstruction.

Image analysis

Imaging data from MDCT and SFDCT of each patient were anonymized and randomly divided into two groups. Images were reconstructed in the axial plane with a section thickness of 1 mm and 3 mm and were laid out side by side in axial planes on one layout. Readers were requested to produce multiplanar reconstructions from the 1 mm raw data and change the window range of the images according to their own requirements for optimal diagnostic assessment.

Images were independently reviewed on a picture archiving and communications system (R11.4.1, Philips, Best, the Netherlands; Sectra, Linkoping, Sweden) by two board-certified neuroradiologists with 13 and 15 years of experience, respectively (EIP and FW). The reviewers were blinded to diagnosis and clinical information and images were assessed with a 4-week time window between the ratings to avoid recall bias.

Readers were asked to rate structures using a 3-point scale (0=not identifiable, 1=identifiable, not diagnostic, 2=diagnostic). The structures rated were: supra- and infratentorial ventricular system, supra- and infratentorial subarachnoid space as well as grey-white matter differentiation of central cortex, basal ganglia, insula and cerebellum. Readers were also asked to rate their confidence in the diagnosis of intracranial hemorrhage, present or not present (subarachnoid, intraventricular or parenchymal) and to provide the Fisher score and identify the ischemic lesions and quantify the Alberta Stroke Program Early CT Scale (ASPECTS). Diagnostic confidence when diagnosing or ruling out a hemorrhage or ischemic lesion was rated using a 3-point grading system (1=low confidence, 2=medium confidenc, 3=high confidence). Finally, readers were asked to subjectively rate the image quality and the effect of the artefacts on diagnostic accuracy.

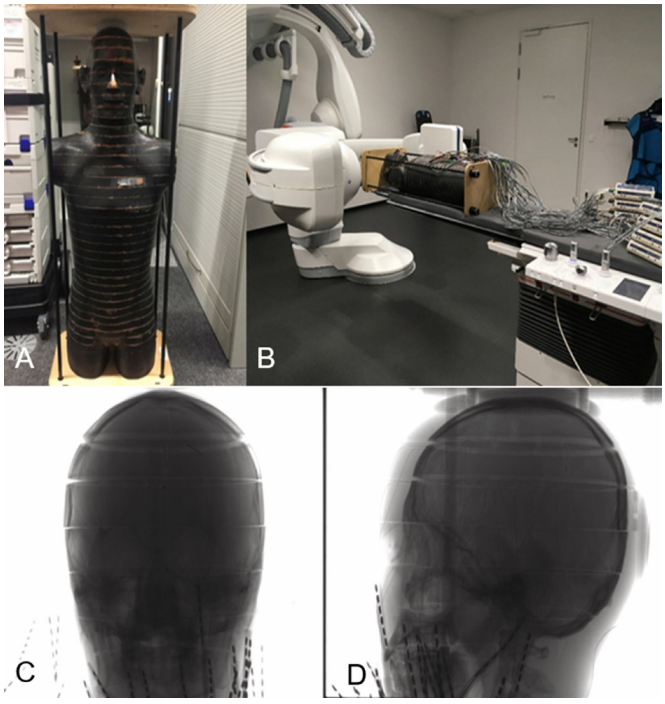

Figure 1 The anthropomorphic Alderson RANDO phantom used for effective dose measurement(A). Phantom standing on the floor and (B) phantom in the experimental set-up for 3D acquisition equipped with MOSFET dosimeters. The position of the head area of the Alderson RANDO phantom being investigated is shown in the frontal view (C) and lateral view (D).

Measurement of effective dose

For angiography systems, the specified regulatory dose parameters are dose-area-product or DAP (μGy*m^2) and air kerma (mGy).[3] The main advantage of using the effective dose is that it allows comparison between different X-ray imaging modalities—for example, cone beam and fan beam CT—and between different imaging protocols. The measurements of effective dose were made with the 7sDCT Sine Spin and 9sDCT Sine Spin Device protocols.

Phantom

An anthropomorphic Alderson RANDO male phantom (The RANDO Phantom, Alderson Research Laboratories, Stanford, Connecticut, USA) was used to evaluate the effective dose (figure 1). This phantom consists of a human skeleton, which is embedded in an isocyanide gum showing the ideal human outer contour. The phantom represents the body of a male human with a height of 173 cm and a body weight of 73.5 kg. This phantom is equipped with slices of 2.5 cm thickness, each having a 1.5 cm × 1.5 cm grid of holes with a diameter of 0.5 cm for holding the dosimeters used to measure the radiation exposure.

Dosimeters

For the assessment of the organ dose, metal oxide semiconductor field-effect transistors (MOSFETs) TN 1002RD-H were used, incorporated into the mobile MOSFET system, model TN-RD-70-W (Best Medical Canada, Ottawa, Ontario, Canada). The mobile MOSFET system consists of remote monitoring dose verification software, a Bluetooth wireless transceiver, and a reader module that acts as a channel between the MOSFETs and the software. Up to five MOSFETs can be connected to one reader. In this study eight readers and 40 MOSFETs were used for simultaneous measurements.

Prior to the measurements, all MOSFET detectors were calibrated. The calibration process has been described in detail elsewhere.[4]

C-arm angiography system

The measurements were performed using the ARTIS icono angiography system (Siemens Healthineers) with a neuro tabletop and a mattress (Siemens Healthcare). The C-arm was positioned head-side and the field of view for 3D imaging was positioned in the head region of the phantom (figure 1). No collimation was applied.

Estimation of effective dose

The MOSFET dosimeters were placed in 38 organ locations in the Alderson RANDO phantom as described by Struffert *et al*.[5] These locations represent the anatomical position of organs (brain, thyroid, lung, bone surface, esophagus, liver, stomach, pancreas, adrenal gland, small intestine, spleen, kidney, red bone marrow, bladder, gonads, etc). Each organ location consists of three measurement points. To fit the MOSFET dosimeters within the phantom's holes, each MOSFET detector was placed into the tissue-equivalent holder.

The 3D imaging protocols were performed three times respectively to reach a sufficient exposure level for the MOSFET detectors before the readings were taken. The organ dose was calculated as the mean value of the measurements for all MOSFET detectors that had been placed in the respective organ sites. For skin and red bone marrow, which are irradiated both by direct and by scattered irradiation, the fraction of directly irradiated organ volume in the head region was taken into account. These data were used to calculate the effective dose according to the guidelines of the International Commission on Radiological Protection (ICRP) 103.[6] The radiation-weighting factor for X-rays was assumed to be 1 in this study, as only photons and electrons were involved.

Statistical analysis

The Wilcoxon test for paired samples was used to compare the different categories of cerebral structures between the SFDCT and the MDCT. Receiver operating characteristic curves were plotted to calculate the area under the curve (AUC) with 95% confidence intervals, sensitivity, specificity, true positive, true negative, false positive and false negative, comparing the diagnostic accuracy considering the CT as the reference. Inter-reader agreement was measured applying the percentage of agreement, Gwet's AC and the Brennan–Prediger coefficient as comparisons. The significance level of the tests was set at 0.05. All statistical analyses were performed using Stata 16.1 (StataCorp, College Station, Texas, USA).

RESULTS

In total, 49 patients were analysed (20 women, 29 men; age range 35–94 years; median age 64.5 years). Median time between MDCT and SFDCT was 7.8 hours (range 30 min–23.5 hours). The rating of cerebral structures showed an equivalent performance of MDCT and SFDCT in terms of diagnostic results for the supratentorial ventricular system (table 1): SFDCT was equivalent to MDCT in 48 out of 49 diagnostic values. However, SFDCT scores were significantly lower than MDCT ($p<0.001$ for all comparisons) for all other cerebral structures such as grey-white matter differentiation in the abovementioned regions and infratentorial ventricular system and subarachnoid spaces. Among these cerebral structures, the second best diagnostic performance was given for the supratentorial subarachnoidal space in 34 (69%) cases with SFDCT, while for MDCT

Table 1 Rating of cerebral structures

Variable		Diagnostic N (%)	Identifiable but not diagnostic N (%)	Not identifiable N (%)	Wilcoxon p value
Supratentorial ventricular system	Sine Spin	48 (98)	1 (2)	0 (0)	
	CT	49 (100)	0 (0)	0 (0)	0.317
Infratentorial ventricular system	Sine Spin	9 (18)	36 (73)	4 (8)	
	CT	48 (98)	1 (2)	0 (0)	<0.001
Supratentorial subarachnoid space	Sine Spin	34 (69)	15 (31)	0 (0)	
	CT	48 (98)	1 (2)	0 (0)	<0.001
Infratentorial subarachnoid space	Sine Spin	5 (10)	23 (47)	21 (43)	
	CT	49 (100)	0 (0)	0 (0)	<0.001
Grey-white differentiation of basal ganglia	Sine Spin	18 (37)	23 (47)	8 (16)	
	CT	47 (96)	2 (4)	0 (0)	<0.001
Grey-white differentiation of insular cortex	Sine Spin	10 (20)	17 (35)	22 (45)	
	CT	46 (94)	2 (4)	1 (2)	<0.001
Grey-white differentiation of central cortex	Sine Spin	29 (59)	16 (33)	4 (8)	
	CT	48 (98)	1 (2)	0 (0)	<0.001
Grey-white differentiation of cerebellum	Sine Spin	1 (2)	7 (14)	41 (84)	
	CT	45 (92)	3 (6)	1 (2)	<0.001

Table 2 Detection of hemorrhage and ischemic lesions

Variable	AUC (95% CI)	Sensitivity (%)	Specificity (%)	TP	TN	FP	FN
Subarachnoid hemorrhage	0.82 (0.71 to 0.93)	84.21	80.00	16	24	6	3
Intraventricular hemorrhage	0.90 (0.79 to 1.00)	83.33	97.30	10	36	1	2
Parenchymal hemorrhage	0.88 (0.77 to 0.98)	75.00	100.00	12	33	0	4
Intracranial hemorrhage	0.92 (0.83 to 1.00)	93.10	90.00	27	18	2	2
Ischaemic lesion	0.84 (0.74 to 0.94)	73.33	94.74	22	18	1	8

AUC, area under the curve; FN, false negative; FP, false positive; TN, true negative; TP, true positive.

the diagnostic performance was 48 (98%) cases. Only one case had diagnostic value in the grey-white matter differentiation of cerebellum with SFDCT compared with 45 (92%) with MDCT.

The detection of subarachnoid, intraventricular and parenchymal hemorrhage and ischemic lesions showed that SFDCT and MDCT performed equally well (table 2). A minimum value of detection for subarachnoid hemorrhage gave a value of 0.82 for the AUC (95% CI 0.71 to 0.93) with sensitivity of 84.2% and specificity of 80.0% and a maximum performance for the intraventricular hemorrhage AUC 0.90 (95% CI 0.79 to 1.00), with a sensitivity and specificity of 83.3% and 97.3%, respectively. SFDCT correctly diagnosed parenchymal hemorrhage in 45 cases with no false positive diagnoses, resulting in 75% sensitivity and 100% specificity. Overall, the correct diagnosis of an intracranial hemorrhage gave a resulting AUC of 0.92 (95% CI 0.83 to 1.00) with sensitivity and specificity of 93.1% and 90.0%, respectively. The diagnosis of ischemic lesion was correct in 40 cases (18 true negative and 22 true positive). There were eight false negatives and one false positive, resulting in 73.3% sensitivity and 94.7% specificity.

For both MDCT and SFDCT, the highest agreement among raters was obtained for the supratentorial ventricular system. Overall, the agreement was good to very good for most of the variables when compared with the MDCT results. However, for some parameters (eg, the infratentorial ventricular system) the agreement among raters in the SFDCT was poor (table 3). Both readers found that artefacts influenced the quality of the image more when obtained with the SFDCT than the MDCT (table 3).

Measurement of effective dose

The calculated effective dose values for the different 3D-imaging protocols (ie, 7sDCT Sine Spin and 9sDCT Sine Spin Device) are summarised in table 4. The accuracy of the measurements was estimated to be ±20%. Accuracy estimates took into account all possible sources of error, such as uncertainty for the reference dosimeter (ionisation chamber), for estimation of the calibration factor for MOSFET detectors used and for calculation of dose for each organ location.

DISCUSSION

Our study shows that the use of SFDCT in preprocedural and postprocedural settings is feasible and allows for the safe diagnosis of intracranial hemorrhage (figure 2) (intraventricular, subarachnoid and intraparenchymal) as well as detection of an early ischemic lesion with high sensitivity and specificity.

Until recently, FDCT was used mainly in assessing acute periprocedural or postprocedural complications in the

Table 3 Agreement among readers

Variable name	Percent of agreement (CT)	Brennan–Prediger (CT)	Gwet's AC	Percent of agreement (Sine Spin)	Brennan–Prediger (Sine Spin)	Gwet's AC
Supratentorial ventricular system	1.000	1.000	1.000	1.000	1.000	1.000
Infratentorial ventricular system	0.939	0.878	0.935	0.327	–0.010	0.038
Supratentorial subarachnoid space	0.980	0.959	0.979	0.816	0.724	0.774
Infratentorial subarachnoid space	0.918	0.878	0.915	0.633	0.449	0.492
Grey-white matter differentiation basal ganglia	0.878	0.755	0.862	0.531	0.296	0.356
Grey-white matter differentiation insula	0.816	0.724	0.799	0.367	0.051	0.099
Grey-white matter central cortex	0.959	0.918	0.957	0.735	0.602	0.652
Grey-white matter cerebellum	0.898	0.847	0.893	0.551	0.327	0.412
Subarachnoid hemorrhage	0.857	0.714	0.730	0.837	0.673	0.680
Diagnostic confidence subarachnoid hemorrhage	0.755	0.633	0.720	0.367	0.051	0.073
Intraventricular hemorrhage	0.857	0.714	0.777	0.980	0.959	0.968
Diagnostic confidence intraventricular hemorrhage	0.837	0.755	0.822	0.469	0.204	0.246
Parenchymal hemorrhage	0.898	0.796	0.811	0.939	0.878	0.898
Intracranial hemorrhage	0.898	0.796	0.801	0.959	0.918	0.921
Diagnostic confidence parenchymal hemorrhage	0.796	0.694	0.771	0.327	–0.010	0.036
Ischemic lesion	0.755	0.510	0.515	0.714	0.429	0.434
Diagnostic confidence ischemic lesion	0.673	0.510	0.577	0.429	0.143	0.167
Artefacts	0.837	0.673	0.784	0.694	0.388	0.392

Table 4 Technical parameters of 3D imaging protocols under investigation and measured effective dose for anthropomorphic Alderson RANDO male phantom for 3D imaging protocols on ARTIS Icono

Parameters of 3D imaging protocols	7sDCT Sine spin
Tube voltage (nominal)	109 kV
Dose/frame (nominal)	1820 nGy/f
Rotation range	220°
Angulation step (degree/frame)	0.4°/f
Effective dose, mSv	2

angiography suite.[7 8] With the new generation of FDCT, the diagnostic accuracy for early ischemic lesions or intracranial hemorrhage is comparable to that of MDCT.[5 9–11] This has potential implications for clinical workflows when acute stroke is suspected—'one-stop shopping concept'[12 13]—as well as in predicting treatment outcomes and in decision making in the acute stroke setting in the angiography suite.[14]

Our results are in line with the findings of Leyhe *et al*[11] showing that SFDCT has high specificity and sensitivity for detecting intracranial hemorrhages. The best diagnostic performance was in detecting intraventricular hemorrhage, followed by intraparenchymal and subarachnoid hemorrhage. High sensitivity and specificity was also shown in detection of ischemic lesions (figure 3) and ASPECTS classification in both MDCT and SFDCT. The eight false negatives and one false positive were attributed to motion artefacts and to metal artefacts in a patient with an aneurysm clipping, respectively.

In contrast to Leyhe *et al*[11] we found a statistically significant difference in diagnostic performance between MDCT and SFDCT in all infratentorial structures (figure 4) and grey-white matter differentiation of the supratentorial and infratentorial structures (figure 3). Only for the supratentorial ventricular system and supratentorial subarachnoid space was the diagnostic performance comparable to MDCT, with no statistically significant differences between the two imaging modalities. The poorer diagnostic performance of SFDCT in grey-white matter differentiation and infratentorial structures is a limitation that needs to be considered in the future development of FDCT and in studies evaluating the diagnostic capability of FDCT in the infratentorial structures. The quality of the images and the diagnostic performance of SFDCT in the presence of artefacts—for example, beam hardening or bone blooming artefacts—was reduced in up to 53% of the cases assessed by reader 1 and up to 38% of those assessed by reader 2. In comparison, the diagnostic performance of MDCT was reduced in only 12% and 16% of the cases compared with SFDCT assessed by reader 1 and reader

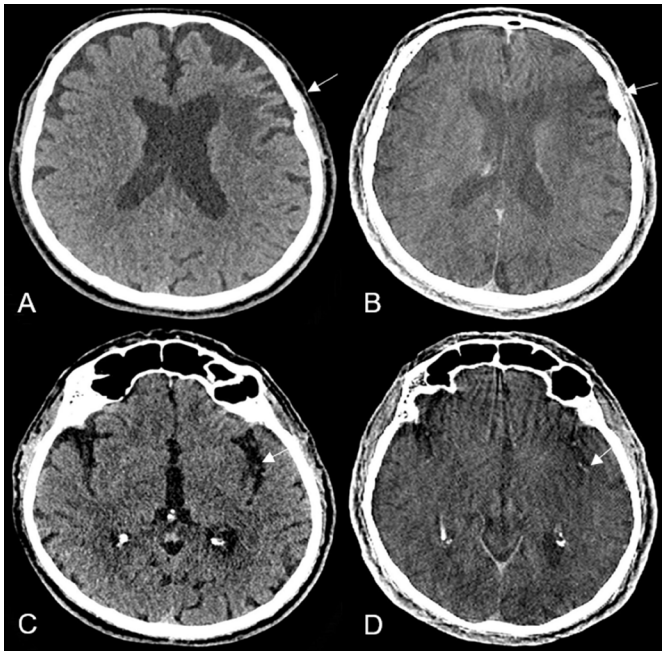

Figure 3 Axial images of a patient with an early ischemic lesion of the left insular cortex and external capsule (white arrow) in MDCT (A) and in FDCT (white arrow) in the angiography suite prior to thrombectomy (B) with occlusion of the left medial cerebral artery. A hemorrhagic transformation of the ischemic lesion was excluded. Axial images of the same patient depicting an older infarction in the territory of the medial cerebral artery in the left frontal lobe (white arrow) in MDCT (C) and in FDCT (D) have a comparable diagnostic accuracy. FDCT, flat detector computed tomography; MDCT, multidetector computed tomography.

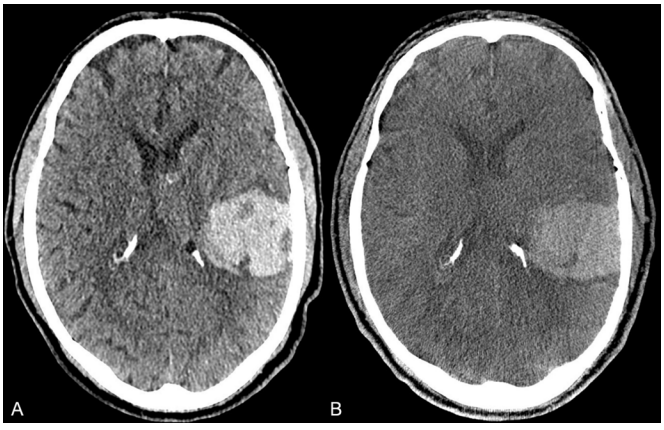

Figure 2 Axial images from a patient with an intraparenchymal hemorrhage of the left parietotemporal lobe in MDCT (A) and follow-up FDCT (B) in the angiography suite prior to conventional angiography to rule out a vascular pathology for the hemorrhage. The margins of the hemorrhage and the perifocal edema are well delineated in the FDCT image. FDCT, flat detector computed tomography; MDCT, multidetector computed tomography.

Figure 4 Axial MDCT (A) and FDCT (B) of a patient with a partially thrombosed aneurysm undergoing a flow-diverter implantation, depicting the infratentorial structures with a reduced delineation of the grey-white matter junction and the subarachnoid spaces in the FDCT image due to beam hardening artefacts. FDCT, flat detector computed tomography; MDCT, multidetector computed tomography.

2, respectively, reflecting the low diagnostic accuracy shown in the infratentorial structures.

Compared with the study by Struffert *et al*,[5] the measurements of effective dose in the Alderson RANDO phantom with the new SFDCT protocol 7sDCT Sine Spin showed a reduction of effective dose for the head scan to 2 mSv from 2.9 mSv measured in the 20 s DR-H brain scan (DR-H DynaCT). Brehm *et al*[15] compared the measurements of effective dose for the head scan measured with the ARTIS Q system to the ARTIS zee biplane system used in the study by Struffert *et al*[5] and showed that there was also a dose reduction for 20sDR Head (2.6 mSv) and 7sDR Head (2.4 mSv) protocols.

The main limitations of our study are its retrospective nature and the non-uniform pathology of the patients examined. Other limiting factors are the time of imaging and the time difference in image acquisition between MDCT and SFDCT, as well as the injection of contrast media if SFDCT was acquired postprocedurally, which could improve the differentiation of the brain structures and the detection of pathological findings. Furthermore, the rate of hemorrhage detection might not be generalizable to patients with suspected acute ischemic stroke as they might have different hemorrhage patterns compared with patients with other hemorrhage etiologies.

Dose measurements

The Alderson RANDO phantom is constructed to represent a wide range of different patients. Therefore, the actual doses to patients might vary from the dose measured in the Alderson RANDO phantom. Nevertheless, the use of an anthropomorphic phantom allows reproducible comparisons between different X-ray imaging modalities, protocols and studies.

CONCLUSIONS

Our findings confirm the high diagnostic sensitivity and specificity of SFDCT in detecting intracranial hemorrhage and early ischemic lesions. In comparison to the previous Sine Spin protocol, we were able to acquire many more images per Sine Spin acquisition with the same dose measurement if not with a tendency toward dose reduction. There are still limitations in delineating grey-white matter differentiation and infratentorial structures in SFDCT.

Acknowledgements The authors gratefully acknowledge the technical support and assistance with phantom experiments of Dr Elizaveta Stepina from Siemens Healthcare GmbH, Forchheim, Germany.

Contributors VDP and PM had full access to all the data in the study and take responsibility for the integrity and accuracy of the data analysis. Study concept and design: VDP and JK. Acquisition of data: TD, EIP, SMP-P, PM. Analysis and interpretation of data: VDP, PM, MB. Drafting of the manuscript: VDP and PM. Critical revision of the manuscript for important intellectual content: FW, JG. Statistical analysis: MB, JK. Administrative, technical, or material support: SMP-P, TD, EIP. Study supervision and guarantor: PM.

Funding The authors have not declared a specific grant for this research from any funding agency in the public, commercial or not-for-profit sectors.

Competing interests None declared.

Patient consent for publication Not applicable.

Ethics approval This study involves human participants and was approved by Kantonale Ethikkomission Bern, KEKBasec PB 018-02023. Participants gave informed consent to participate in the study before taking part.

Provenance and peer review Not commissioned; externally peer reviewed.

Data availability statement Data are available upon reasonable request.

ORCID iDs
Johannes Kaesmacher http://orcid.org/0000-0002-9177-2289
Eike I Piechowiak http://orcid.org/0000-0001-5609-0998
Tomas Dobrocky http://orcid.org/0000-0002-6167-3343

REFERENCES

1 Kak AC, Slaney M. *Principles of computerized tomographic imaging*. IEEE Press, 1988.
2 Strobel N, Meissner O, Boese J. 3D Imaging with flat-detector C-arm systems. In: Reiser MF, Becker CR, Nikolaou K, eds. *Multislice CT*. Berlin, Heidelberg: Springer, 2009: 33–51.
3 International Electrotechnical Commission. IEC 60601-2-43:2010/AMD2:2019 Amendment 2 - Medical electrical equipment - Part 2-43: Particular requirements for the basic safety and essential performance of X-ray equipment for interventional procedures; 2019. https://webstore.iec.ch/publication/65930
4 Roser P, Birkhold A, Zhong X, *et al*. Pitfalls in interventional X-ray organ dose assessment-combined experimental and computational phantom study: application to prostatic artery embolization. *Int J Comput Assist Radiol Surg* 2019;14:1859–69.
5 Struffert T, Hauer M, Banckwitz R, *et al*. Effective dose to patient measurements in flat-detector and multislice computed tomography: a comparison of applications in neuroradiology. *Eur Radiol* 2014;24:1257–65.
6 ICRP. The 2007 recommendations of the International Commission on Radiological Protection. Ann ICRP 2 ICRP Publication; 2007. https://www.icrp.org/docs/ICRP_Publication_103-Annals_of_the_ICRP_37(2-4)-Free_extract.pdf
7 Psychogios M-N, Buhk J-H, Schramm P, *et al*. Feasibility of angiographic CT in peri-interventional diagnostic imaging: a comparative study with multidetector CT. *AJNR Am J Neuroradiol* 2010;31:1226–31.
8 Doerfler A, Gölitz P, Engelhorn T, *et al*. Flat-panel computed tomography (DYNA-CT) in neuroradiology. from high-resolution imaging of implants to one-stop-shopping for acute stroke. *Clin Neuroradiol* 2015;25(Suppl 2):291–7.
9 Maier IL, Leyhe JR, Tsogkas I, *et al*. Diagnosing early ischemic changes with the latest-generation flat detector CT: a comparative study with multidetector CT. *AJNR Am J Neuroradiol* 2018;39:881–6.
10 Frölich AM, Buhk J-H, Fiehler J, *et al*. Voxel-based sensitivity of flat-panel CT for the detection of intracranial hemorrhage: comparison to multi-detector CT. *PLoS One* 2016;11:e0165794.
11 Leyhe JR, Tsogkas I, Hesse AC, *et al*. Latest generation of flat detector CT as a peri-interventional diagnostic tool: a comparative study with multidetector CT. *J Neurointerv Surg* 2017;9:1253–7.
12 Bouslama M, Haussen DC, Grossberg JA, *et al*. Flat-panel detector CT assessment in stroke to reduce times to intra-arterial treatment: a study of multiphase computed tomography angiography in the angiography suite to bypass conventional imaging. *Int J Stroke* 2021;16:1–10.
13 Psychogios M-N, Behme D, Schregel K, *et al*. One-stop management of acute stroke patients: minimizing door-to-reperfusion times. *Stroke* 2017;48:3152–5.
14 Chen L, Xu Y, Shen R, *et al*. Flat panel CT scanning is helpful in predicting hemorrhagic transformation in acute ischemic stroke patients undergoing endovascular thrombectomy. *Biomed Res Int* 2021;2021:1–8.
15 Brehm A, Stamm G, Lüpke M, *et al*. Effective dose to patient measurements for flat-detector computed tomography protocols in acute stroke care. *Eur Radiol* 2020;30:5082–8.